Plastoquinol diffusion in linear photosynthetic electron transport

Rowan Mitchell, Andreas Spillmann, and Wolfgang Haehnel
Lehrstuhl für Biochemie der Pflanzen, Westfälische Wilhelms-Universität, Münster, Federal Republic of Germany

ABSTRACT The diffusion of plastoquinol and its binding to the cytochrome bf complex, which occurs during linear photosynthetic electron transport and is analogous to reaction sequences found in most energy-converting membranes, has been studied in intact thylakoid membranes. The flash-induced electron transfer between the laterally separated photosystems II and photosystems I was measured by following the sigmoidal reduction kinetics of $P\text{-}700^+$ after previous oxidation of the intersystem electron carriers. The amount of flash-induced plastoquinol produced at photosystem II was (*a*) reduced by inhibition with dichlorophenyl-dimethylurea and (*b*) increased by giving a second saturating flash. These signals were simulated by a new model which combines a deterministic simulation of reaction kinetics with a Monte Carlo approach to the diffusion of plastoquinol, taking into account the known structural features of the thylakoid membrane. The plastoquinol molecules were assumed to be oxidized by either a diffusion-limited or a nondiffusion-limited step in a collisional mechanism or after binding to the cytochrome bf complex. The model was able to account for the experimental observations with a nondiffusion-limited collisional mechanism or with a binding mechanism, giving minimum values for the diffusion coefficient of plastoquinol of 2×10^{-8} cm^2s^{-1} and 3×10^{-7} cm^2s^{-1}, respectively.

INTRODUCTION

Photosynthetic electron transport of higher plants involves the integral complexes of photosystem (PS) II, cytochrome bf, and PS I, which operate in series via plastoquinone and plastocyanin. In higher plants PS I and functional PS II are restricted to the nonappressed stroma and the appressed grana regions of thylakoid membranes, respectively (1–3), whereas the cytochrome bf complexes are almost homogeneously distributed (4, 5). The electrons produced by PS II must be transported over the relatively large distance of up to 300 nm between the two membrane regions to reach PS I. The electron transport is carried out between PS II and cytochrome bf complexes by diffusion of plastoquinol within the lipid bilayer of thylakoid membrane and between the cytochrome bf complexes and PS I by diffusion of plastocyanin in the thylakoid lumen. Recently, we have shown a lateral heterogeneity in the distribution of plastocyanin and its light-induced diffusion from stroma to grana regions (6). Plastoquinone is approximately evenly distributed in both thylakoid regions (7). The problem of diffusing plastoquinol and its oxidation at the cytochrome bf complex is equivalent to that of ubiquinol diffusion and its oxidation at the cytochrome bc_1 complex in bacterial and mitochondrial electron transport. However, the lateral separation of the complexes in grana and stroma membrane regions may provide the possibility to study in situ a contribution of the diffusion which may not be observed at the short distances of the complexes in other membranes.

A long-range electron transport by diffusion of plastoquinol has been discussed using simply the averaged distance between the two photosystems and Einstein's equation (8) for the diffusion in two dimensions giving the mean square of the displacement x as a function of time and the diffusion coefficient D,

$$\langle x^2 \rangle = 4Dt. \quad (1)$$

The value of t chosen depends on whether plastoquinol diffusion is assumed to be involved in the rate determining oxidation of plastoquinol or in a faster preceding reaction. Due to this uncertainty, estimates for the lateral diffusion coefficient D lie in the extremely wide range of 10^{-9}–10^{-6} cm^2s^{-1} (9–12). In functional membranes the long-range lateral diffusion is obstructed by the dispersed membrane proteins and the macroscopically observed diffusion coefficient may be by an order of magnitude smaller than in pure lipid membranes (13, 14). The low value of 3×10^{-9} cm^2s^{-1} reported for the long-range diffusion of an ubiquinone analogue in mitochondrial inner membrane provided the basis for a model of the electron transport

Address correspondence to W. Haehnel, Lehrstuhl für Biochemie der Pflanzen, Westfälische Wilhelms-Universität, Hindenburgplatz 55, D-4400 Münster, FRG.

Dr. Mitchell's present address is Biochemistry and Physiology Department, AFRC Institute of Arable Crops Research, Rothamsted Experimental Station, Harpenden, Herts AL5 2JQ, England.

0006-3495/90/10/1011/14 $2.00

where the lateral diffusion of ubiquinol is the rate-limiting step (15, 16). However, determinations of the lateral diffusion coefficient of the ubiquinone analogue and of ubiquinone incorporated into lipid membranes yielded values of 2×10^{-8} (16, 17) and $>10^{-6}$ cm^2s^{-1} (18) by measurements of fluorescence recovery after bleaching and of fluorescence quenching of probes, respectively. This difference in the diffusion coefficient is not understood, but may partially be due to problems arising from probe specific effects (19). We have used a different approach to the problem of long-range diffusion by using undisturbed thylakoid membranes.

However, the contribution of the diffusion to reaction kinetics of the electron transport is not only determined by the diffusion coefficient of plastoquinol but also by the probability of the reaction to take place on the encounter between plastoquinol and the cytochrome bf complex. In a diffusion-controlled process a reaction takes place on every encounter resulting in a reaction rate which is critically dependent on the path length of diffusion. Therefore, the heterogeneous distribution of the complexes in the thylakoids would be reflected in the kinetics of a reaction only if the process is completely or partially diffusion controlled.

Our approach to the role of the diffusion of plastoquinol has been to follow the reduction of P-700, the reaction center chlorophyll of PS I, by electrons induced by a flash at PS II as a convenient method of accurately measuring full-chain electron transport. The half-time of the sigmoidal reduction kinetics and the initial lag give information about the rate-determining oxidation of plastoquinol (20) and reactions preceding this step (21), respectively. The rate of the step which involves the plastoquinol diffusion can be varied by the amount of plastoquinol produced by flash excitation either by inhibition of PS II with dichlorophenyl-dimethylurea (DCMU) or by using a second flash immediately after the first one. The size of the differences in kinetic parameters due to the varied plastoquinol concentration can only be estimated with the aid of a model which takes into account the diffusion process. It is not possible to solve the diffusion equation for the thylakoid membrane except for the oversimplified models given in our preliminary report (22) or for the diffusion of protons at the surface (23).

The Monte Carlo method was introduced by Metropolis et al. (24) as a sampling algorithm to investigate properties of interacting individual molecules in terms of a rigid-sphere system and has been extended to a broad range of physical systems (25). This algorithm has also been used to simulate diffusion in biomembranes for a variety of problems (14, 26). Generally one starts from a description of a system in terms of a model and uses random numbers to construct the appropriate probability which is used to create a Markov chain of new states. The subsequent configurations may be associated with a scale of time which can be used to solve the diffusion equation for complex boundary conditions. We have used this approach to study the photosynthetic electron transport in thylakoids by combining it with differential equations describing the deterministic reaction kinetics. Multiples of the step width in time used in the numerical integration of the differential equations were chosen to match with the time attributed to a step in the Monte Carlo approach. It is this combination which helps to study biological reaction sequences starting in a protein complex then followed by diffusion of a substrate across considerable distances before the reaction sequence continues in the next multienzyme complex. We have applied this technique to the diffusion of plastoquinol, taking into account the sizes and arrangement of the thylakoid protein complexes (for reviews cf. references 10 and 27), and combined it with iterative simulations of the other reactions to build a complete model of linear photosynthetic electron transport. We have included two cases for the mechanism of plastoquinol oxidation; a collisional mechanism which implies an oxidation of plastoquinol immediately on a successful encounter with a cytochrome bf complex and a tight-binding mechanism which includes an irreversible binding of plastoquinol to the Q_Z site of the cytochrome bf complex before its slow oxidation takes place. Both mechanisms have been used to compare a diffusion-limited and a nondiffusion-limited reaction of plastoquinol with our experimental data.

MATERIALS AND METHODS

Thylakoid isolation

Thylakoids were isolated from spinach leaves as described (21). The 1-cm cuvette contained chloroplasts at 9 μM chlorophyll, 100 mM D-Sorbitol, 10 mM 4-(2-hydroxyethyl)-1-piperazineethanesulphonic acid (Hepes)/KOH, pH 7.5, 5 mM $MgCl_2$, 100 μM methyl viologen, and 2 μM gramicidin D. Chlorophylls were determined spectrophotometrically in 80% acetone extract (28).

Spectroscopy

The flash-induced kinetics of P-700 were measured at 705 nm as previously described (21), except that a transient recorder (DL912; Data Laboratories, Mitcham, Surrey, England) was used, and that the signals were averaged and analyzed in a minicomputer (A700; Hewlett-Packard, Cupertino, CA). The continuous far-red measuring light of 1.4 Wm^{-2} ensured that all the components between the two photosystems were oxidized between flashes, except for cytochrome b and a fraction of P-700 (21). The electrical bandwidth was from d.c. to 10 kHz. Blue (filter BG 23/6 mm; Schott F, Glaswerke, Mainz, West-Germany) flashes with 2 μs full-width half maximum (model 6100; Photochemical Research Associates, London, Ontario) of saturating energy of 600 μJ were used for excitation. The content of the cuvette was changed every 50 flashes. The flash frequency, transient recorder dwell time, and number of averaged signals used are given in the figure legends.

We found that differences occurred in the kinetics between different chloroplast preparations, but that the kinetics measured at varied conditions showed the same trends within a single preparation. The curves shown are corrected for flash-induced fluorescence artifacts measured immediately after the recording of the signal with the same sample in the absence of measuring light. The lag parameter of the $P\text{-}700^+$ reduction kinetics was defined as the X intercept of a tangent drawn through the point of inflection on the curve. The level of the lag gives that of fully oxidized P-700. The amplitude of P-700 reduction was determined either measuring the reduced level after a shutter-controlled illumination with blue light of 150 Wm^{-2} for 40 ms, giving the total amount of P-700, or after a single flash by fitting the latter part of the time course assuming a first-order reoxidation of P-700 to the steady-state level.

Simulations

Model simulations were written in FORTRAN77 and carried out on a minicomputer (A700; Hewlett-Packard) with a vector processor card. The program allows interactive selection of all structural parameters of the membrane model under graphic control. The random number generator provided as library routine was used for the Monte Carlo simulations after having been tested for uniformity of distribution. First- and second-order steps were simulated iteratively using the method of finite differences (29) with a maximum step time of 2.5 μs.

Description of model

The model was composed of two parts: an iterative simulation of reactions using first- and second-order rate equations, and a Monte Carlo simulation of the diffusion of plastoquinol and its interaction with cytochrome bf complexes. The output of the model is the relative concentration of reduced P-700.

Reactions simulated using differential equations

Table 1 lists the electron-carrying species that were considered in the model and their starting concentrations. Plastoquinone is termed Q_B, Q_Z, or Q_C if it is bound to PS II, the oxidizing site of the cytochrome bf complex or its reducing site, respectively. The initial concentrations are based on a 1:1:2:1 stoichiometry for PS II/cytochrome bf/plastocyanin/PS I (30). Under our steady-state conditions the acceptors of PS II function as a two-electron gate (31). Therefore, after a flash approximately one half of the acceptors will stay in the state $Q_AQ_B^-$ while the other half produces plastoquinol after the initial formation of $Q_A^-\ Q_B^-$.

A problem of the simulation is to include the complex reactions at the cytochrome bf complex. The most commonly accepted scheme for the oxidation of plastoquinol is that it is a concerted two-electron process, in which one electron passes onto the two b cytochromes and one to the P-700 donors via the Rieske iron sulfur protein (FeS). If there was already an electron on the b cytochromes, the two electrons on the b cytochromes combine to reduce a plastoquinone molecule (32–34). It was therefore necessary to consider three states of the cytochrome b subunit with zero, one, or two electrons on the b cytochromes. If the state with one reduced cytochrome b is stable within our measuring time (32, 34) which is consistent with the finding that the electrons produced by a flash at PS II go quantitatively through to P-700 and its electron donors under our conditions within 200 ms (35), we must assume that every other cytochrome bf complex has one cytochrome b reduced before the flash. This is in line with the observation that one quarter of cytochrome b is reduced in the steady state (34). The other intersystem components are oxidized before the flash (35).

TABLE 1 Initial concentrations relative to total P-700 after far-red preillumination

Abbreviation	Species	Initial concentration
$Q_A^-Q_B^-$	reduced Q_A and plastosemiquinone bound to PS II	0.5*
$Q_AQ_B^{2-}$	Q_A and plastoquinol dianion bound to PS II	0
PQH_2	freely diffusing plastoquinol	0
BF	cytochrome bf complex with both cytochrome b oxidized	0.5
BF^-	cytochrome bf complex with one cytochrome b oxidized	0.5
BF^{2-}	cytochrome bf complex with neither cytochrome b oxidized	0
Q_ZH_2	plastoquinol bound to the oxidizing site of the cytochrome bf complex	0
FeS_{OX}	oxidized Rieske iron sulfur (FeS) center	1
Cyt-f_{OX}	oxidized cytochrome f	1
Pc_{OX}	oxidized plastocyanin	2
$P\text{-}700^+$	oxidized P-700	1

*The initial concentration of $Q_A^-Q_B^-$ was varied according to the amount of active PS II in the experiment being simulated.
The ratios of $(Q_A + Q_A^-)/(BF + BF^- + BF^{2-})/(Pc + Pc_{OX})/(P\text{-}700 + P\text{-}700^+)$ were 1:1:2:1, where each cytochrome bf complex consists of 2 cytochrome b, 1 Rieske iron sulfur center, and 1 cytochrome f (60).

Table 2 gives a schematic list of the reactions that are included in the model. To simplify the model some fast steps for which the exact kinetics are not known are considered implicitly with these reactions. These are the following: the reduction of Q_A occurs too rapidly (36) to affect the output of the model. The protonation of Q_B^{2-} and its subsequent release from PS II were taken as one step with a constant k_2. The rate constant k_4 of the plastoquinone reduction in the Q-cycle by two reduced cytochromes b (37) includes also the release from the binding site after formation of plastoquinol. The time for the transfer of electrons from cytochrome f to P-700 was simulated as being due to the electron transfer from plastocyanin to P-700. This latter simplification allowed us to assume that the Rieske FeS center, cytochrome f, and plastocyanin are in constant equilibrium. Our experience with more complex models suggests that these simplifications do not significantly alter the output of the model.

Rate constants taken from the literature are $k_1 = 1{,}150\ s^{-1}$ (20, 21) and $k_5 = 2{,}800\ s^{-1}$ from the halftime of 270 μs for the oxidation of cytochrome f by $P\text{-}700^+$ (38). The rate constant for the back reaction $k_{-5} = 12\ s^{-1}$ between plastocyanin and P-700 was calculated assuming redox potentials of 340 and 480 mV, respectively (39). All concentrations are expressed as amounts relative to the amount of P-700, so that although k_3, k_3', k_5, and k_{-5} are second order, they also have units of $seconds^{-1}$. The values of redox potentials depend on measuring conditions (40), but the large proportion of electrons which pass through to P-700 after a saturating flash under oxidizing conditions indicate a large difference in potential between P-700 and its donors (32, 35). The diffusion, binding, and oxidation of plastoquinol and the reduction of Q_c (reactions 3–6 in Table 2) are not unambiguously attributable to known details of reaction kinetics, so that the values of D, P, k_3, k_3', and k_4 have

TABLE 2 Processes considered in the model of electron transport

	Reaction		Method of simulation
1	$Q_A^-Q_B^-$	$\xrightarrow{k_1}$ $Q_AQ_B^{2-}$	$-d[Q_A^-Q_B^-]/dt = k_1 \times [Q_A^-Q_B^-]$
2	$Q_AQ_B^{2-} + 2H^+$	$\xrightarrow{k_2}$ $PQH_2 + Q_A$	$-d[Q_AQ_B^{2-}]/dt = k_2 \times [Q_AQ_B^{2-}]$
3	PQH_2	$\xrightarrow{PQH_2 \text{ diffusion}}$ Q_ZH_2	diffusion coefficient D / binding probability P } Monte Carlo
4*	Q_ZH_2-BF + FeS_{OX}	$\xrightarrow{k_3}$ $BF^- + FeS_{red} + PQ + 2H^+$	$-d[Q_ZH_2\text{-}BF]/dt = k_3 \times [Q_ZH_2\text{-}BF] \times [FeS_{ox}]$
5*	Q_ZH_2-BF^- + FeS_{ox}	$\xrightarrow{k_3'}$ $BF^{2-} + FeS_{red} + PQ + 2H^+$	$-d[Q_ZH_2\text{-}BF^-]/dt = k_3' \times [Q_ZH_2\text{-}BF^-] \times [FeS_{ox}]$
6	$BF^{2-} + PQ + 2H^+$	$\xrightarrow{k_4}$ $BF + PQH_2$	$-d[BF^{2-}]/dt = k_4 \times [BF^{2-}]$
7	FeS_{red} + (Cyt-f + Pc)$_{ox}$	$\rightleftharpoons$ FeS_{OX} + (Cyt-f + Pc)$_{red}$	$K = \frac{[FeS_{ox}] \times [(Cyt\text{-}f + Pc)_{red}]}{[FeS_{red}] \times [(Cyt\text{-}f + Pc)_{ox}]}$
8	$Pc_{red} + P\text{-}700^+$	$\underset{k_{-5}}{\overset{k_5}{\rightleftharpoons}}$ $Pc_{ox} + P\text{-}700$	$-d[P\text{-}700^+]/dt = k_5 \times [Pc_{red}] \times [P\text{-}700^+] - k_{-5} \times [Pc_{OX}] \times [P\text{-}700]$

Where: $[Pc_{red}]/[Pc_{ox}] = [(Cyt\text{-}f + Pc)_{red}]/[(Cyt\text{-}f + Pc)_{ox}]$.
*These processes were assumed to be instantaneous in the collisional mechanism.

to be treated as unknowns. For the sake of simplicity, we assume that the oxidation of Q_ZH_2 has the same rate constant regardless of whether there is a reduced cytochrome b on the cytochrome bf complex. k_3 is therefore taken to be equal to k_3' throughout.

Simulation of diffusion of plastoquinol by a Monte Carlo method

The diffusion of plastoquinol and its interaction with the cytochrome bf complex was simulated in a Monte Carlo algorithm, in which random numbers were used to simulate the diffusion of plastoquinol molecules in a two-dimensional model, which represented the structure of the thylakoid and the size and distribution of the integral membrane complexes. The simulation of plastoquinol diffusion was built on a number of assumptions which are listed below.

Model of thylakoid membranes

In the model representing a stacked thylakoid of higher plants (Fig. 1 *A*), it was assumed that:

(*a*) 40% of the area of the thylakoid membrane is in the granal region (41).

(*b*) 50% of the circumference of the granal region connects with the stromal region via six equally sized, equally spaced strips (fret regions) (27). The regions on the circumference between these strips represent a barrier to diffusion.

(*c*) The radius of the granum is 220 nm (27).

(*d*) PS II complexes are located only in the granal regions, PS I and ATP synthase complexes are restricted to the stromal regions (3, 27, 42, 43), while cytochrome bf complexes are homogeneously distributed between the two regions (4, 5).

(*e*) The average area of thylakoid membrane per PS II complex in the granal region is 710 nm^2 (44).

(*f*) Protein complexes are distributed in a hexagonal arrangement at maximum separation of complexes from the same type (2).

(*g*) The stoichiometry of the complexes PS II/cytochrome bf/PS I/ATP synthase is 1:1:1:1.5 (27, 30).

(*h*) The radii of the complexes are 8, 4, 6, and 5 nm for PS II with its light harvesting chlorophyll proteins (45), cytochrome bf (5), PS I (46), and ATP synthase (27), respectively.

(*i*) The protein complexes are effectively immobile, as diffusion coefficients measured for complexes are generally too low to have significant effects within the considered time scales (e.g., a value of 4×10^{-10} cm^2s^{-1} was determined for the cytochrome bc_1 complex [15]).

Monte Carlo algorithm

(*a*) At the start of the simulation, plastoquinol molecules are positioned at a random point on the circumference of a PS II complex. In a simulation of a saturating flash, every other PS II complex produces a plastoquinol (see above). For simulations of measurements made with DCMU-inhibited samples, the number of plastoquinol molecules were reduced to correspond with the measured level of inhibition. Dual flash experiments were simulated as follows: after a single saturating flash simulated as above, an interval corresponding to 2.04 ms followed before a second lot of plastoquinol is produced. These plastoquinol molecules are positioned at PS II complexes which did not produce plastoquinol in the first flash. The number of plastoquinol molecules produced in the second flash is set as determined experimentally.

(*b*) Plastoquinol molecules start to move only after a simulated release from PS II. The kinetics of this release are determined by a numerical simulation of a sequence of two first-order processes (Table 2, steps 1 and 2).

(*c*) In each iteration of the model (termed "walk"), the plastoquinol molecules are moved by 1 nm, corresponding approximately to the distance between lipid molecules in the membrane (47, 48). This movement took place in one of six equally probable directions spaced at 60° intervals, selected by a random number. This results in movement in a trigonal lattice and is shown for one plastoquinol molecule in Fig. 1 *B*.

(*d*) If plastoquinol encounters a complex or a boundary, one of the other possible directions for movement is selected, except at a cytochrome bf complex.

(*e*) Encounters between plastoquinol and cytochrome bf complexes which have their single Q_Z-binding site unoccupied and have at least one oxidized cytochrome b are counted. Every $1/P$ of such encounters

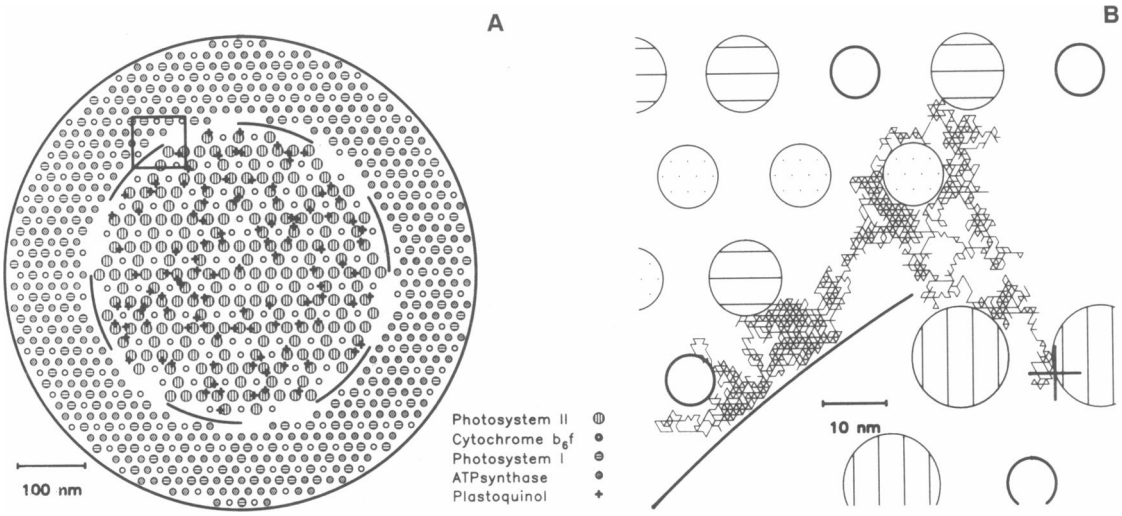

FIGURE 1 (*A*) Representation of the thylakoid membrane used by the Monte Carlo algorithm to simulate the diffusion of plastoquinol. The outer circle represents the edge of the thylakoid, whereas the inner, broken circle represents the edge of the granum. The space between complexes and boundaries represents the lipid bilayer in which the plastoquinol diffuses. The box delimits the expanded area of the map shown in *B*. (*B*) Expansion of box in *A*. A diffusion path as generated by the Monte Carlo algorithm for a single plastoquinol molecule is shown, with the starting position at a PS II designated by a +. The path shown consists of 2110 steps. In this case, binding (indicated by a *) occurred on the fifth encounter between the plastoquinol and a cytochrome bf complex.

results in binding, where P is the preset binding probability. If binding occurs, this plastoquinol molecule is removed from the set of freely diffusing plastoquinol.

(*f*) In the tight-binding mechanism, the Q_ZH_2 remains until oxidation occurs by reactions 4 and 5 in Table 2. In the collisional mechanism, oxidation is considered to occur instantaneously. Following oxidation of Q_ZH_2, the status of the cytochrome bf is changed to indicate one more reduced cytochrome b and the number of electrons in the FeS $\rightleftharpoons$ cyt f $\rightleftharpoons$ Pc equilibrium is increased by one.

(*g*) For both mechanisms, the reduction of plastoquinone at the cytochrome bf complexes was simulated assuming a first-order dependence on the number of cytochrome bf complexes with two reduced b cytochromes. When a reduction of a plastoquinone molecule occurs, a plastoquinol appears at the circumference of the cytochrome bf complex and is added to the set of freely diffusing plastoquinol. The cytochrome bf complex is flagged as having both cytochrome b oxidized.

(*h*) The time represented by each walk of the algorithm was given by:

$$t = X^2/(4D), \qquad (2)$$

where t is the time per walk, X is the step length of 1 nm, and D is the diffusion coefficient in the absence of protein. The validity of this equation was checked by comparing the output of the Monte-Carlo algorithm with a closed solution for a simple diffusion problem (22).

RESULTS

Experiments

Determination of amount of electrons produced by photosystem II and the ratio of the photosystems

The kinetics of P-700$^+$ reduction were measured under conditions which varied the amount of electrons produced by PS II. This parameter can be conveniently determined with the P-700 signal by using a longer measurement period. After a short flash of saturating energy the area bound by the transient reduction of P-700$^+$ at continuous far-red light of constant intensity is proportional to the number of electrons generated at PS II (49, 50). Therefore, the area a_I in the presence of inhibitor over the area a_C of the control gives the fraction of noninhibited PS II. Such P-700 signals are shown in Fig. 2 which were used to determine an inhibition of 71% of PS II by 50 nM DCMU. The amplitude ΔA_I of the signal in the presence of DCMU (Fig. 2 *B*) was 29% of that found for total P-700 after a long flash ΔA_{tot} (not shown). Owing to this low amount of reduced P-700 it is safe to assume that almost all electrons from PS II have reduced P-700 and a negligible fraction of the electron donors of PS I, as a result of the equilibrium constant being considerably greater than 1 (see above) and in agreement with the reduction of 91% of total P-700 in the absence of inhibitor in Fig. 2. From these data we accurately determine the ratio of the functionally connected PS II and PS I

$$n_{PSII}/n_{PSI} = (\Delta A_I/\Delta A_{tot})/(a_I/a_C) \qquad (3)$$

as 1.0. This approach only uses three measurements with one sample at 705 nm and does not need corrections for inhomogeneous absorption by the chloroplast suspension or the assumption of an extinction coefficient. A correction for the misses which always occur in PS II (51) and for double hits with our flash lamp in the range of +5% is

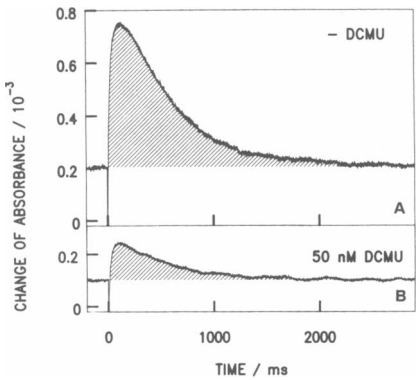

FIGURE 2 The change of absorbance of 705 nm due to the reduction and reoxidation of P-700 after a saturating flash. The shaded area is proportional to the total number of electrons produced at PS II at constant intensity of the monitoring light. The flash frequency was 0.2 Hz, the dwell time was 1 ms per address. Other conditions were as described in the Materials and Methods. (*A*) Signal measured from a sample in the absence of DCMU. Average of 50 flashes. (*B*) Signal measured from a sample in the presence of 50 nM DCMU. Average of 150 flashes.

estimated from the O_2 oscillation in successive flashes (not shown).

Kinetics with varied amount of plastoquinol

Fig. 3 shows two P-700 signals over 20 ms measured in the presence and absence of 50 nM DCMU. For comparison, the curves are scaled by the factor determined in Fig. 2 for the number of electrons produced in each case. Over the first millisecond, the two signals show slight differences, possibly due to imperfect correction for the flash-induced artifact. After this time the two normalized signals exhibit no detectable differences in kinetics except for a slightly higher amplitude of the signal in the presence of DCMU which is consistent with the equilibrium discussed.

The P-700 absorbance change induced by two saturating flashes 2.04 ms apart is shown in Fig. 4 *B*. This signal can be regarded as a composite of two P-700 reduction time courses due to the two flashes. When a single flash signal measured in the same sample (*A*) is subtracted off the two-flash signal (*B*), the resulting trace (*B-A*) represents the kinetics of full-chain electron transport of the electrons attributable to the second flash. This subtracted curve is only shown as a convenient way of comparing the early kinetics of $P\text{-}700^+$ reduction after single and second flashes. The number of electrons produced were determined from the areas under the curves using the same method as in Fig. 2, showing that the second flash induces 85% of the electrons which are produced with a single flash. This difference is due to those PS II complexes in which the electron transfer from Q_A^- to Q_B has not taken place during the 2.04 ms between the flashes. Although the value of 85% is lower than that expected from the halftime of 200 μs found by chlorophyll fluorescence measurements for this reaction (52) it has been found consistently in our experiments. A comparison of the

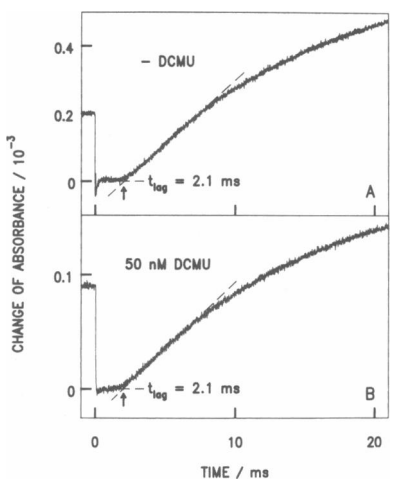

FIGURE 3 The reduction of P-700 after a saturating flash as a function of time. The flash frequency was 0.2 Hz and the dwell time was 10 μs per address. The number of flashes used in the two measurements was chosen so as to give similar signal-to-noise ratios. (*A*) Signal measured from a sample in the absence of DCMU. Average of 150 flashes. (*B*) Signal measured from a sample in the presence of 50 nM DCMU. Average of 3150 flashes.

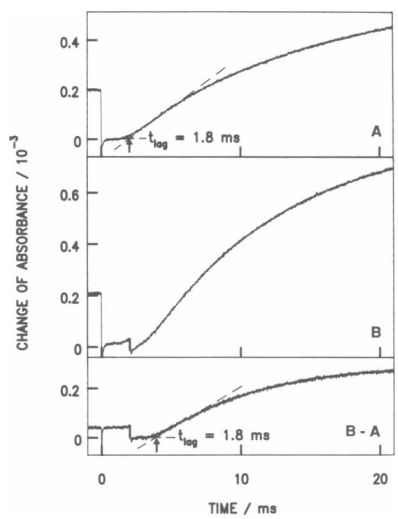

FIGURE 4 (*A*) The reduction of P-700 after a saturating flash as a function of time. (*B*) The reduction of P-700 after two saturating flashes, 2.04 ms apart. (*B-A*) The result of subtracting signal A from signal B. Average of 300 flashes with a flash frequency of 0.2 Hz. The dwell time was 10 μs per address.

single and second flash signals (Figs. 4, *A* and *B-A*) after normalization to the amount of electrons produced shows that the kinetics are similar over the first 10 ms, but at longer times the second flash signal lies increasingly lower than the single flash curve. As a result, the lag parameters of the single and second flash signals can be compared directly, but the halftimes cannot. There is no significant difference in the lags measured in the single and second flash signals.

Modeling

To obtain quantitative information about the nature of plastoquinol diffusion and its interaction with the cytochrome bf complex from these data, our model was used with one of two mechanisms; collisional or tight-binding at the Q_Z site. For each mechanism, near diffusion-limited and nondiffusion-limited cases were simulated; i.e., the value of the probability P of binding with a cytochrome bf complex on encounter was set to 0.25 or 0.005, respectively. We have chosen $P = 0.25$ because it seems unlikely that plastoquinol hits the single binding site on every encounter, but have also tested simulations with $P = 1$. For convenience, we refer to the near diffusion-limited case with $P = 0.25$ as diffusion limited.

The model parameters for which values were not known (k_2, k_3, k_4, and D for the tight-binding mechanism; k_2, k_4, and D for the collisional mechanism) were varied across a range of values until a good approximation to the signal being simulated was obtained. The long computing time needed for the simulations generated by the model with the Monte Carlo algorithm precluded the use of nonlinear regression for parameter optimization. However, for the nondiffusion-limited cases, the Monte Carlo simulation of binding can be substituted with a second-order rate equation (see Discussion), which enabled us to optimize the parameter values by nonlinear regression. The parameters were then used in the model with the Monte Carlo algorithm. The results of varying parameters are shown in Figs. 5–7, where simulations using ranges of values for D or for $t_4 = \ln 2/k_4$ are plotted together with the normalized single flash signal shown in Fig. 4 *A*. The best fit of a given signal is indicated by the lowest value for the root mean square of the residuals (given in the figure legends). It can be seen that while changes in fast steps affected predominantly the lag phase, changes in the oxidation of plastoquinol affected the main kinetics and changes in k_4 changed the kinetics in the latter part of the simulation (Figs. 5 and 6). The optimal values of the parameters obtained for both control signals in Fig. 3 *A* and Fig. 4 *A* are listed in Table 3.

For the tight-binding mechanism, two of the floated parameters, k_2 and D, affected primarily only the length of the lag, so that it was only possible to obtain minimum

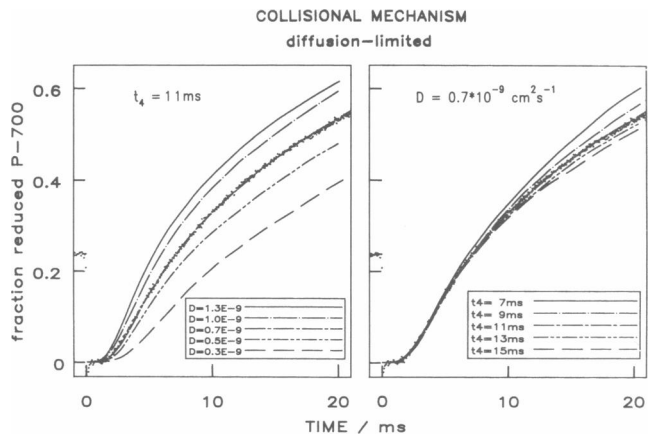

FIGURE 5 Comparison of the output of the model using the diffusion-limited collisional mechanism (*lines*) with the observed P-700 signal (*points*). The signal is the control shown in Fig. 4 *A* normalized to the absorbance change for complete P-700 reduction. The left-hand figure shows simulations from the model for a range of values for the diffusion coefficient (D) as shown in the key, with the value of t_4 set to 11 ms. The right hand figure shows simulations with D fixed at 7×10^{-10} cm^{2}s^{-1}, for a range of values of t_4, as shown in the key. Other parameter values, which were the same for all the lines shown, are listed in Table 3. The root mean square of the residuals for the best simulation shown was 3.8×10^{-3}.

values for them from the optimization process. The optimized values shown in Table 3 for the tight-binding mechanism are those obtained with D set equal to 3×10^{-7} cm^{2}s^{-1}.

The fact that it is possible to obtain a good approximation to the signal with the model with either mechanism

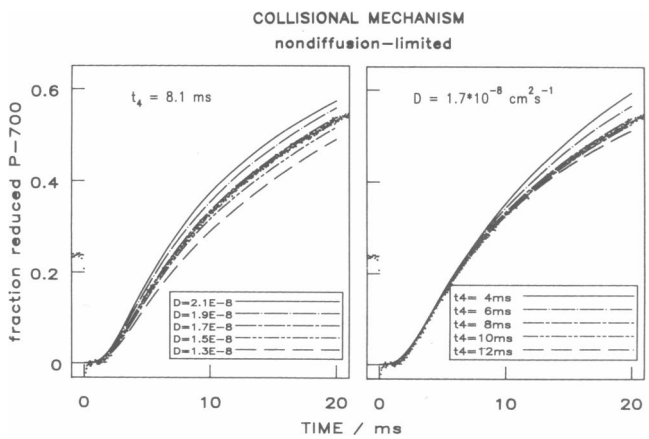

FIGURE 6 Equivalent to Fig. 5, but with output from the model with the nondiffusion-limited collisional mechanism. To obtain simulations with this mechanism which approximate well to the signal, similar values for t_4 but a considerably different range of values for D from those in Fig. 5 were used. The root mean square of the residuals for the best simulation shown was 6.2×10^{-3}.

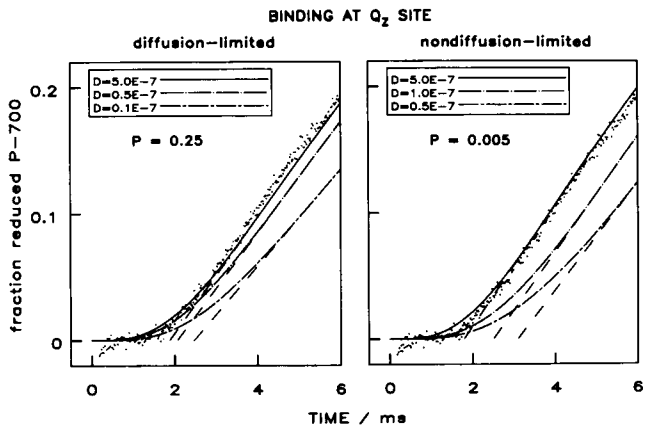

FIGURE 7 Comparison of output from the model with tight binding at Q_Z (*continuous and dash-dotted lines*) with the single flash signal (same as Fig. 4 *A*, shown as points), for a range of values of *D*. The left- and right-hand diagrams show near diffusion-limited and nondiffusion-limited simulations, respectively. The dashed lines are the tangents at the point of inflection and indicate the lag as intercept of the time axis. The root mean square of the residuals for the best simulation shown was 4.7×10^{-3} and 5.0×10^{-3} for the diffusion-limited and nondiffusion-limited cases, respectively.

and assuming either diffusion limitation or nondiffusion limitation (Figs. 5–7), shows that simple comparison of the output with a single signal is an inadequate test of the model. The next stage was therefore to see whether the model is capable of accurately simulating a double-flash or DCMU-inhibited P-700 reduction curve with the values obtained by optimizing to the corresponding control signal (Table 3).

For the tight-binding mechanism only a minimum value of *D* can be obtained by simulation of the control signals (Fig. 7), the simulations of the dual-flash and DCMU-inhibited signals with this mechanism were also carried out over a range of values for *D*. Fig. 8 shows how the lags of simulations of single, second flash, and DCMU-inhibited curves decrease asymptotically with increasing *D*, for both diffusion-limited and nondiffusion-limited cases. As *D* is increased, the differences between the lags of the simulations of the three signals decrease until they become negligible at $D \geq 3 \times 10^{-7}\ \mathrm{cm^2 s^{-1}}$. This corresponds to the experimental situation, where the lags of the DCMU-inhibited signal (Fig. 3 *B*) and of the second-flash signal (Fig. 4 *B-A*) do not differ from those of their corresponding controls (Fig. 3 *A* and Fig. 4 *A*, respectively).

Fig. 9 *A* shows collisional mechanism simulations of a dual-flash experiment together with the dual-flash signal from Fig. 4 *B*. It can be seen that, while both simulations

TABLE 3 Optimal parameter values for single-flash signals

Mechanism		*P*	Parameter	Control Fig. 3 *A*	Control Fig. 4 *A*
tight binding mechanism	diffusion limited	0.25	k_2	$495\ s^{-1}$	$865\ s^{-1}$
			D^*	$3.0 \times 10^{-7}\ cm^2 s^{-1}$	$3.0 \times 10^{-7}\ cm^2 s^{-1}$
			k_3	$165\ s^{-1}$	$151\ s^{-1}$
			k_4	$82\ s^{-1}$	$82\ s^{-1}$
	nondiffusion limited	0.005	k_2	$990\ s^{-1}$	$2{,}310\ s^{-1}$
			D^*	$3.0 \times 10^{-7}\ cm^2 s^{-1}$	$3.0 \times 10^{-7}\ cm^2 s^{-1}$
			k_3	$147\ s^{-1}$	$151\ s^{-1}$
			k_4	$100\ s^{-1}$	$82\ s^{-1}$
collisional mechanism	diffusion limited	0.25	k_2	$495\ s^{-1}$	$865\ s^{-1}$
			D	$7.1 \times 10^{-10}\ cm^2 s^{-1}$	$7.0 \times 10^{-10}\ cm^2 s^{-1}$
			k_4	$73\ s^{-1}$	$63\ s^{-1}$
	nondiffusion limited	0.005	k_2	$495\ s^{-1}$	$865\ s^{-1}$
			D	$1.8 \times 10^{-8}\ cm^2 s^{-1}$	$1.7 \times 10^{-8}\ cm^2 s^{-1}$
			k_4	$85\ s^{-1}$	$86\ s^{-1}$

*D was set to this value and k_2 adjusted to obtain the observed lag.

Fixed parameters:

$k_1 = 1{,}550\ \mathrm{s^{-1}}$.

$E°$ of FeS, cytochrome f, plastocyanin, P-700 were 320, 340, 340, 480 mV, respectively.

$k_5 = 2{,}800\ \mathrm{s^{-1}}$.

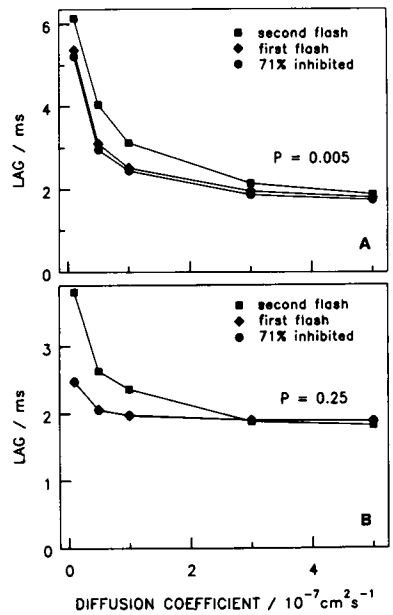

FIGURE 8 Lags of simulations generated with the tight binding mechanism at Q_Z with various values of the diffusion coefficient; (*A*) nondiffusion-limited mechanism; (*B*) diffusion-limited mechanism. Lags are shown for simulations of a single flash (■) (as indicated by the dashed lines shown in Fig. 7), a second flash (■), and a single flash (●) with 71% of PS II inhibited. The second flash simulation was generated by subtracting a simulation of a single flash off a simulation of a double flash as shown for the signals in Fig. 4. The experimentally observed lag was 1.8 ms (see Fig. 4).

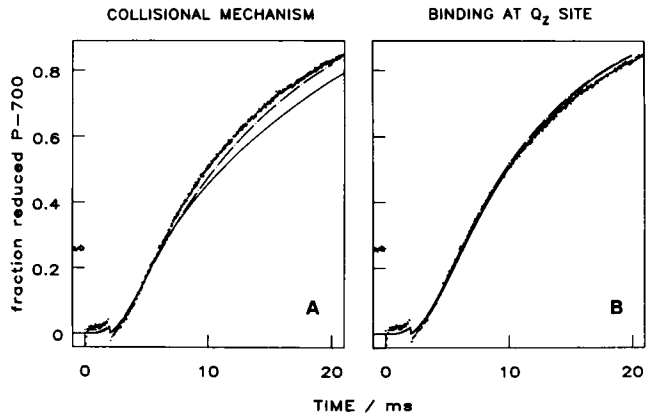

FIGURE 9 Comparison of normalized dual flash signal (same as Fig. 4 *B*, shown as points) with simulations of a dual flash signal from the model using the collisional (*A*) and tight binding mechanism (*B*); each for the diffusion limited (*solid lines*) and nondiffusion-limited (*dash-dotted lines*) cases. The values of the parameters used in the model were those obtained by optimizing the simulation of the single flash control signal (Fig. 4 *A*), as shown in Figs. 5–7, and are listed in Table 3. The root mean square of the residuals: (*A*) 5.3×10^{-2} and 3.0×10^{-2} for diffusion-limited and nondiffusion-limited case, respectively; (*B*) 3.0×10^{-2} and 2.4×10^{-2} for diffusion-limited and nondiffusion-limited case, respectively.

lie below the signal, the nondiffusion-limited simulation is the better approximation. Fig. 9 *B* is an equivalent figure, but for simulations using the tight-binding mechanism. There is little difference between the diffusion-limited and nondiffusion-limited cases, and here both simulations lie above the signal, in contrast to the collisional mechanism simulations. However, both the simulations in Fig. 9 *B* are reasonably good approximations to the signal.

In Fig. 10, the DCMU-inhibited signal (Fig. 3 *A*) is compared with simulations of this signal generated by using the parameter values from the fitting of its control and assuming 71% inhibition of PS II. For the collisional mechanism simulations (Fig. 10 *A*), the nondiffusion-limited case is a better approximation than the diffusion-limited one, which lies above the signal. Both the curves generated with the model using the tight-binding mechanism simulate the signal reasonably accurately (Fig. 10 *B*).

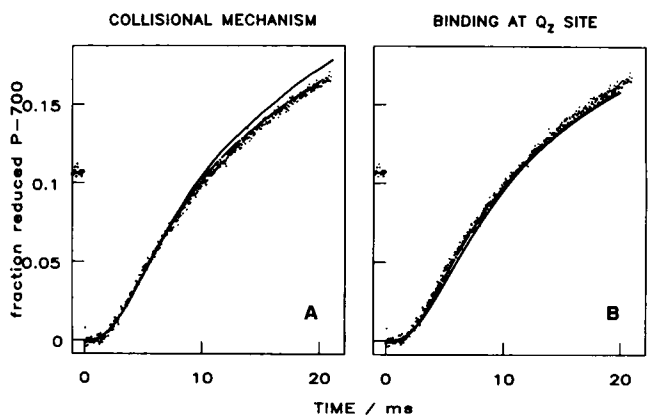

FIGURE 10 Comparison of normalized signal measured in the presence of DCMU (same as Fig. 3 *B*, shown as points) with simulations assuming 71% inhibition of PS II (*lines*). Simulations were generated using the collisional (*A*) and the tight binding mechanisms (*B*); each for the diffusion-limited (*solid lines*) and nondiffusion-limited (*dash-dotted lines*) cases. The values of the parameters used in the model were those obtained by optimizing the simulation of the uninhibited control signal (Fig. 3 *A*), and are listed in Table 3. The root mean square of the residuals: (*A*) 6.0×10^{-3} and 2.6×10^{-3} for diffusion-limited and nondiffusion-limited case, respectively; (*B*) 4.4×10^{-3} and 2.8×10^{-3} for diffusion-limited and nondiffusion-limited case, respectively.

DISCUSSION

The work here addressed questions concerning the lateral diffusion of plastoquinol and the mechanism of its binding

and oxidation by the cytochrome bf complex. Related aspects are the magnitude of the diffusion coefficient of plastoquinol, the identity of the rate-limiting reaction and the contribution of the Q-cycle to the reactions of linear electron transport. The electron transfer steps are essential for our understanding of the long-range electron transport, but have only been investigated in vivo in a few studies. Our approach was to construct a model with which the signal of the electron transfer from PS II to PS I after a single flash was fitted using different mechanisms for the diffusion of plastoquinol and its binding to the cytochrome bf complex, and to see which of these mechanisms best explained the signals observed when the amount of flash-induced plastoquinol is varied experimentally.

Fitting of model to single flash signals

For the control signals shown in Fig. 3 *A* and Fig. 4 *A* the parameters of the model with the different mechanisms were varied until values were obtained which gave a good approximation of the signal. When nondiffusion-limited cases are considered, binding of plastoquinol is equally likely at all cytochrome bf complexes available for binding, and the signals can be fitted by nonlinear regression after substitution of the Monte Carlo algorithm with a second-order rate equation. The rate of binding $(\mathrm{d}[PQH_2]/\mathrm{d}t)_{\mathrm{bind}}$ is given by

$$(\mathrm{d}[PQH_2]/dt)_{\mathrm{bind}} = -k_{\mathrm{bind}}[PQH_2][BF + BF^-], \quad (4)$$

where $[PQH_2]$ is the concentration of free plastoquinol, $[BF + BF^-]$ the concentration of cytochrome bf complexes available for binding, both expressed relative to the amount of P-700, and k_{bind} is the second-order rate constant given by

$$k_{\mathrm{bind}} = cPn_{\mathrm{PSI}}/(\ell^2 t), \quad (5)$$

where t is the time per walk given in Eq. 2 in Materials and Methods, c is the number of trigonal lattice points adjacent to the circumference of a cytochrome bf complex, n_{PSI} is the number of PS I (i.e., the number of P-700) in the model thylakoid, and ℓ is the total number of lattice points in the model thylakoid. From Eqs. 2 and 5, k_{bind} is proportional to the product $D \times P$ for the nondiffusion-limited case. That the Monte Carlo algorithm produces the same output as Eq. 4 can be used as a criterion of nondiffusion-limitation; in our model, this was satisfied with $P \leq 0.005$.

Figs. 5–7 show how the simulations vary with the D and k_4 parameters in comparison with the control signal from the dual-flash experiment. For the tight-binding mechanism, the lag is determined by two unknown parameters, k_2 and D, so that they do not have unique optimal values, and the values shown for k_2 in Table 3 are those with D set to 3×10^{-7} $\mathrm{cm^2 s^{-1}}$.

The control signals (shown in Fig. 3 *A* and Fig. 4 *A*) were carried out on different preparations of thylakoids. The slight differences in lags and halftimes are within the range of values that are commonly observed in spinach thylakoid preparations. The slightly different values for the k_2, k_3, k_4, and D parameters as obtained by the optimization process are given in Table 3. The reason for this variation is not known, but environmental factors such as growth temperature are known to affect the lipid to protein ratio in the thylakoid membrane, for example (53).

Contribution of Q-cycle

The time course of P-700$^+$ reduction 10 ms after the flash rises too slowly to be modeled by a simple chain of first-order reactions (54), nor can it be fully accounted for by the back reactions which occur between the Rieske iron sulfur protein, cytochrome f, plastocyanin, and P-700 as a consequence of their redox potentials. For all the mechanisms considered in our model, the adoption of a mandatory Q-cycle with a halftime for the reduction and release of plastoquinone at the Q_C site of the order of 8 ms was necessary to successfully simulate the whole kinetics of P-700$^+$ reduction. After every Q-cycle half of the amount of plastoquinol being oxidized at the Q_Z site is released again at the Q_C site which slows down the transfer of the total amount of electrons from PS II to PS I.

Modeling of inhibited PS II and dual-flash signals

Consequences of tight-binding mechanism

In the tight-binding mechanism, the diffusion of plastoquinol precedes its slow oxidation and therefore affects the lag phase of the P-700$^+$ reduction kinetics. It is in particular this mechanism which should result in distinct differences in the kinetics at different amounts of plastoquinol. The more plastoquinol is present, the less free binding sites at cytochrome bf complexes are available, and the longer the lag. The binding sites of cytochrome bf complexes near to PS II complexes tend to be occupied first, so that in the case of the dual flash, most of the molecules generated in the second flash would be forced to diffuse into the stromal region in this model. This effect can be seen in Fig. 8, where for values of $D \leq 10^{-7}$ $\mathrm{cm^2}$ $\mathrm{s^{-1}}$, there is a substantial difference in the lag phase of simulations between those for second and first flashes. The difference between the DCMU-inhibited and first

flash simulations is less pronounced, because tight-binding sites are in excess for both.

However, the experimental observation is that the lag phase is not altered by the amount of flash-induced plastoquinol because no significant difference is seen between the lags of signals after inhibition of PS II (Fig. 3) nor after the second flash (Fig. 4). This situation is only approached when D is increased so that the influence of the binding step on the lag diminishes. For $D \geq 3 \times 10^{-7}$ cm^2s^{-1} the difference in lags for both diffusion-limited and nondiffusion-limited cases is within the precision of our measurement. The fact that the lags of the simulations converge to a lag of 2.1 ms is simply a reflection of the value chosen for k_2, but the value of D at which they converge is independent of this choice. Thus, a tight-binding mechanism would only be consistent with our data if the diffusion coefficient of plastoquinol is $>3 \times 10^{-7}$ cm^2s^{-1}.

Consequences of a collisional mechanism

For the collisional mechanism, the rate-limiting oxidation of plastoquinol occurs by diffusion and is controlled by the binding probability at the cytochrome bf complex, so that the whole kinetics are affected by the diffusion process. As the oxidation of plastoquinol proceeds, there is an accumulation of cytochrome bf which cannot oxidize plastoquinol, because both cytochromes b are reduced due to the slow reduction of Q_C. This fraction of cytochrome bf increases at the increased plastoquinol concentration after a second flash and slows down the oxidation of plastoquinol. As compared with this second-order process the intramolecular, first-order oxidation of plastoquinol after its binding to the cytochrome bf complex in the tight-binding mechanism is much less changed by this effect. Thus, the model predicts slower kinetics for the dual-flash signal with the collisional mechanism than with the tight-binding mechanism (data not shown).

This effect is more pronounced with the diffusion-limited than with the nondiffusion-limited collisional mechanism in the dual flash signal, where the cytochrome bf complexes in the granal region are more likely to have both cytochrome b reduced after the first flash than those in the stromal region, so that plastoquinol produced by the second flash must diffuse into the stromal region or wait for the reduction of Q_C before it can be oxidized. This can be seen by the much slower kinetics predicted by the diffusion-limited collisional mechanism for the dual-flash signal (Fig. 9 *A*) and slightly faster kinetics for the inhibited PS II signal (Fig. 10 *A*) as compared with the nondiffusion-limited case. In fact, the magnitude of the effect of varying the amount of plastoquinol predicted by the diffusion-limited case is greater than that which is observed experimentally, while the nondiffusion-limited case simulations fit the signals reasonably well (Fig. 9 *A* and Fig. 10 *A*). It is remarkable that the diffusion coefficient did not have to be greater than 2×10^{-8} cm^2s^{-1} to describe our data with this mechanism.

Diffusion coefficient

The values for the diffusion coefficient D that can be obtained using our model are dependent on the value that is used for the binding probability P. We set $P = 0.25$ for a nearly diffusion-limited case, taking account a limited reaction site at the surface of the cytochrome bf complex. If a value of $P = 1$ is used, the value of D needed to fit a single-flash signal using the collisional mechanism is 20% lower than that listed in Table 3 for $P = 0.25$. In the nondiffusion-limited collisional mechanism the second-order rate constant is proportional to $D \times P$ (see above) and D can have any value provided that P is small enough to avoid limitation by diffusion. The maximum value of P for which this is true was found to be 0.005, which yields a value of 2×10^{-8} cm^2s^{-1} for D. This value is similar to the diffusion coefficient of lipid molecules in bilayers (17). It is considerably lower than all previous estimates which took into account that the rate-limiting step in photosynthetic electron transport is not diffusion limited.

For both the tight-binding and collisional mechanisms, only a minimum value of D can be estimated. For tight-binding, this is the value of 3×10^{-7} cm^2s^{-1} at which diffusion ceases to have any influence on the kinetics because it is so rapid. The value of D in our model relates to the rate of plastoquinol diffusion that would be seen in the membrane without protein obstacles (14). As such it can be best related to direct measurements of quinone diffusion coefficients made in protein-free liposomes. Values of 10^{-6}–10^{-5} cm^2s^{-1} were obtained for the diffusion coefficient of ubiquinone in phospholipid liposomes by a fluorescence quenching technique (18, 55). More recently, Blackwell et al. (19) have determined values of 1.3–3.5×10^{-7} cm^2s^{-1} for the diffusion of plastoquinol in phosphatidylcholine vesicles using a different fluorescence quenching method. The same authors recalculated the diffusion coefficient of ubiquinone using the data of reference 55, arriving at a value of 2.5×10^{-7} cm^2s^{-1}. However, the presence of protein almost certainly decreases the fluidity of the membrane, as has been shown by reconstituting the isolated CF_0 complex of the chloroplast ATP synthase into vesicles composed of thylakoid lipids (56), so that these values represent an upper limit for D in our model, where we consider diffusion in the thylakoid membrane. For this reason, the minimum value of 3×10^{-7} cm^2s^{-1} for D required by the model with the tight-binding mechanism seems rather high.

Comparing mechanisms

There is some positive evidence from other work that plastoquinol oxidation occurs by a collisional mechanism. The mechanism of the analogous reaction of ubiquinol oxidation by the cytochrome bc_1 complex in *Rhodobacter spheroides* has been studied in some detail (57, 58). The kinetics of the reaction as a function of ubiquinol concentration in membranes depleted of endogenous ubiquinol was consistent with a collisional mechanism in this system (57). In another study the pre-steady-state kinetics of the oxidation of duroquinol by isolated reduced cytochrome bf complexes were found to be second order as would be expected under these circumstances for a collisional mechanism (59).

Wang et al. (58) investigated the possibility that the oxidation of ubiquinol is diffusion limited in *Rhodobacter spheroides*. The kinetics of the reduction of cytochrome b-561 were measured at a range of temperatures and the low activation energy obtained was taken as indicating that the reaction is not diffusion limited. However, recently a high temperature dependence of the viscosity of lipid membranes has been found (16).

Another possible mechanism for the oxidation of plastoquinol would be a reversible rapid binding at Q_Z, followed by slower oxidation, as has been suggested for ubiquinol oxidation in *Rhodobacter sphaeroides* (61). This could be modeled by adding an unbinding step to the tight-binding mechanism, so that values of D as high or higher than that obtained for that mechanism would be required to give the observed kinetics.

An obvious extension of the work presented here is to measure the kinetics of P-700 reduction under conditions which induce unfolding of the thylakoid membranes and a homogeneous distribution of the photosystems. In these circumstances, if the oxidation of plastoquinol is diffusion limited the difference in kinetics between the second and first flash in a dual flash experiment would be expected to be less than that observed here using stacked thylakoid membranes. However, the results of such experiments do not support the operation of a diffusion-limited mechanism (Spillmann, A., R. Mitchell, H. Robenek, and W. Haehnel, manuscript in preparation).

In conclusion, the results are best fitted by our model assuming either a very rapid tight-binding step for the oxidation of plastoquinol and a diffusion coefficient $\geq 3 \times 10^{-7}$ cm^2s^{-1} or a nondiffusion-limited collisional mechanism and a low value of the diffusion coefficient of $\geq 2 \times 10^{-8}$ cm^2s^{-1}. In our view, the data presented here and elsewhere is best accounted for by the nondiffusion-limited collisional mechanism.

The exact nature of the contribution of the diffusion of plastoquinol to the kinetics of photosynthetic electron transfer is very difficult to determine by experiment alone because there is at present no way of accurately measuring the steps in which it is involved. Our alternative approach in which the whole-chain kinetics, which can be very accurately determined, were successfully modeled has enabled us to set new lower limits for the possible values of D and to exclude a diffusion-limited collisional mechanism. Due to the number of uncertainties which still remain regarding the structure and functioning of the thylakoid system, we have not investigated all of the possible alternative assumptions for the model, for example, it has recently been suggested that there is inhomogeneity in the distribution of plastoquinone (62). However, an advantage of our approach is that as experimental evidence accumulates, the model may be modified and the consequences for kinetics investigated.

Financial support by the Deutsche Forschungsgemeinschaft (SFB 171-A3) is gratefully acknowledged. Dr. Mitchell was supported by a fellowship from the European Molecular Biology Organization.

Received for publication 4 January 1990 and in final form 30 May 1990.

REFERENCES

1. Andersson, B., and J. M. Anderson. 1980. Lateral heterogeneity in the distribution of chlorophyll-protein complexes of the thylakoid membranes of spinach chloroplasts. *Biochim. Biophys. Acta.* 593:427–440.
2. Barber, J. 1986. Surface electrical charges and protein phosphorylation. *In* Encyclopedia of Plant Physiology, New Series, Photosynthesis III. L. A. Staehelin and C. J. Arntzen, editors. Springer-Verlag, Berlin. 19:653–664.
3. Staehelin, L. A., and M. DeWit. 1984. Correlation of structure and function of chloroplast membranes at the supramolecular level. *J. Cell. Biochem.* 24:261–269.
4. Allred, D. R., and L. A. Staehelin. 1986. Spatial organization of the cytochrome b_6-f complex within chloroplast thylakoid membranes. *Biochim. Biophys. Acta.* 849:94–103.
5. Olive, J., O. Vallon, F.-A. Wollman, M. Recouvreur, and P. Bennoun. 1986. Studies on the cytochrome b6-f complex. II. Localization of the complex in the thylakoid membranes from spinach and Chlamydomonas reinhardtii by immunocytochemistry and freeze-fracture analysis of b6-f mutants. *Biochim. Biophys. Acta.* 851:239–248.
6. Haehnel, W., R. Ratajczak, and H. Robenek. 1989. Lateral distribution and diffusion of plastocyanin in chloroplast thylakoids. *J. Cell Biol.* 108:1397–1405.
7. Chapman, D. J., and J. Barber. 1986. Analysis of plastoquinone-9 levels in appressed and non-appressed thylakoid membrane regions. *Biochim. Biophys. Acta.* 850:170–172.
8. Einstein, A. 1906. Zur Theorie der Brownschen Bewegung. *Ann. d. Physik.* 19:371–381.
9. Cramer, W. A., and A. R. Crofts. 1982. Electron and proton transport. *In* Photosynthesis, Energy Conversion by Plants and Bacteria. Govindjee, editor. Academic Press, New York. 1:387–467.
10. Haehnel, W. 1984. Photosynthetic electron transport in higher plants. *Annu. Rev. Plant Physiol.* 35:659–693.

11. Millner, P. A., and J. Barber. 1984. Plastoquinone as a mobile redox carrier in the photosynthetic membrane. *FEBS (Fed. Eur. Biochem. Soc.) Lett.* 169:1–6.
12. Whitmarsh, J. 1986. Mobile electron carriers in thylakoids. *In* Encyclopedia of Plant Physiology, New Series, Photosynthesis III, Photosynthetic Membranes and Light Harvesting Systems. L. A. Staehelin and C. J. Arntzen, editors. Springer-Verlag, Berlin. 19:508–527.
13. Eisinger, J., J. Flores, and W. P. Petersen. 1986. A milling crowd model for local and long-range obstructed lateral diffusion. Mobility of excimeric probes in the membrane of intact erythrocytes. *Biophys. J.* 49:987–1001.
14. Saxton, M. J. 1987. Lateral diffusion in an archipelago: the effect of mobile obstacles. *Biophys. J.* 52:989–997.
15. Gupte, S., E.-S. Wu, L. Hoechli, M. Hoechli, K. Jacobson, A. Sowers, and C. R. Hackenbrock. 1984. Relationship between lateral diffusion, collision frequency, and electron transfer of mitochondrial inner membrane oxidation-reduction components. *Proc. Natl. Acad. Sci. USA.* 81:2606–2610.
16. Chazotte, B., and C. R. Hackenbrock. 1989. Lateral diffusion as a rate-limiting step in ubiquinone-mediated mitochondrial electron transport. *J. Biol. Chem.* 264:4978–4985.
17. Chazotte, B., and C. R. Hackenbrock. 1988. The multicollisional, obstructed, long-range diffusional nature of mitochondrial electron transport. *J. Biol. Chem.* 263:14359–14367.
18. Fato, R., M. Battino, G. P. Castelli, and G. Lenaz. 1985. Measurement of the lateral diffusion coefficients of ubiquinones in lipid vesicles by fluorescence quenching of 12-(9-Anthroyl)-Stearate. *FEBS (Fed. Eur. Biochem. Soc.) Lett.* 179:238–242.
19. Blackwell, M. F., K. Gounaris, S. Zara, and J. Barber. 1987. A method for estimating lateral diffusion coefficients in membranes from steady-state fluorescence quenching studies. *Biophys. J.* 51:735–744.
20. Stiehl, H. H., and H. T. Witt. 1969. Quantitative treatment of the function of plastoquinone in photosynthesis. *Z. Naturforschg.* 24:1588–1598.
21. Haehnel, W. 1976. The reduction kinetics of chlorophyll a_1 as an indicator for proton uptake between the light reactions in chloroplasts. *Biochim. Biophys. Acta.* 440:506–521.
22. Haehnel, W., R. Mitchell, and A. Spillmann. 1987. Lateral electron transport in thylakoids of higher plants. *In* Progress in Photosynthesis Research. J. Biggins, editor. Martinus Nijhoff, Dordrecht, The Netherlands. 2:513–520.
23. Junge, W., and A. Polle. 1986. Theory of proton flow along appressed thylakoid membranes under both non-stationary and stationary conditions. *Biochim. Biophys. Acta.* 848:265–273.
24. Metropolis, N., A. W. Rosenbluth, M. N. Rosenbluth, A. H. Teller, and E. Teller. 1953. Equation of state calculations by fast computing machines. *J. Chem. Phys.* 21:1087–1092.
25. Binder, K. 1987. Applications of the Monte Carlo Method in Statistical Physics. Springer-Verlag, Berlin. 341 pp.
26. Pink, D. A., D. Laidlaw, and D. M. Chisholm. 1986. Protein lateral movement in lipid bilayers. Monte Carlo simulation studies of its dependence upon attractive protein-protein-interactions. *Biochim. Biophys. Acta.* 863:9–17.
27. Staehelin, L. A. 1986. Chloroplast structure and supramolecular organization of photosynthetic membranes. *In* Encyclopedia of Plant Physiology, New Series, Photosynthesis III, Photosynthetic Membranes and Light Harvesting Systems. L. A. Staehelin and C. J. Arntzen, editors. Springer-Verlag, Berlin. 19:1–84.
28. Porra, R. J., W. A. Thompson, and P. E. Kriedemann. 1989. Determination of accurate extinction coefficients and simultaneous equations for assaying chlorophylls a and b extracted with four different solvents: verification of the concentration of chlorophyll standards by atomic absorption spectroscopy. *Biochim. Biophys. Acta.* 975:384–394.
29. Bard, A. J., and L. R. Faulkner. 1980. Electrochemical Methods. John Wiley and Sons, New York. 675–697.
30. Whitmarsh, J., and D. R. Ort. 1984. Stoichiometries of electron transport complexes in spinach chloroplasts. *Arch. Biochem. Biophys.* 231:378–389.
31. Wraight, C. A. 1981. Oxidation-reduction physical chemistry of the acceptor quinone complex in bacterial photosynthetic reaction centers: evidence for a new model of herbicide activity. *Isr. J. Chem.* 21:348–354.
32. Joliot, P., and A. Joliot. 1984. Electron transfer between the two photosystems. I. Flash excitation under oxidizing conditions. *Biochim. Biophys. Acta.* 765:210–218.
33. Rich, P. R. 1988. A critical examination of the supposed variable proton stoichiometry of the chloroplast cytochrome bf complex. *Biochim. Biophys. Acta.* 932:33–42.
34. Rich, P. R., P. Heathcote, and D. A. Moss. 1987. Kinetic studies of electron transfer in a hybrid system constructed from the cytochrome bf complex and photosystem I. *Biochim. Biophys. Acta.* 892:138–151.
35. Haehnel, W. 1973. Electron transport between plastoquinone and chlorophyll-a_1 in chloroplasts. *Biochim. Biophys. Acta.* 305:618–631.
36. Trissl, H.-W., U. Kunze, and W. Junge. 1982. Extremely fast photoelectric signals from suspensions of broken chloroplasts and of isolated chromatophores. *Biochim. Biophys. Acta.* 682:364–377.
37. Mitchell, P. 1976. Possible molecular mechanisms of the protonmotive function of cytochrome systems. *J. Theor. Biol.* 62:327–367.
38. Haehnel, W., A. Pröpper, and H. Krause. 1980. Evidence for complexed plastocyanin as the immediate electron donor of P-700. *Biochim. Biophys. Acta.* 593:384–399.
39. Malkin, R. 1982. Redox properties and functional aspects of electron carriers in chloroplast photosynthesis. *In* Electron Transport and Photophosphorylation. J. Barber, editor. Elsevier Biomedical Press, Amsterdam. 1–47.
40. Joliot, P., and A. Joliot. 1984. Electron transfer between the two photosystems. II. Equilibrium constants. *Biochim. Biophys. Acta.* 765:219–226.
41. Berzborn, R. J., D. Müller, P. Roos, and B. Andersson. 1981. Significance of different quantitative determinations of photosynthetic ATP-synthase CF1 for heterogeneous CF1 distribution and grana formation. *In* Photosynthesis III. Structure and Molecular Organization of the Photosynthetic Apparatus. G. Akoyunoglou, editor. Balaban International Science Services, Philadelphia, PA. 107–120.
42. Andersson, B., and J. M. Anderson. 1985. The chloroplast thylakoid membrane—isolation, subfractionation and purification of its supramolecular complexes. *In* Modern Methods of Plant Analysis, New Series, Cell Components. H. F. Linskens and J. F. Jackson, editors. Springer-Verlag, Berlin. 1:231–258.
43. Bohner, H., H. Böhme, and P. Böger. 1980. Reciprocal formation of plastocyanin and cytochrome c-553 and the influence of cupric ions on photosynthetic electron transport. *Biochim. Biophys. Acta.* 592:103–112.
44. Simpson, D. J. 1981. The ultrastructure of barley thylakoid membranes. *In* Photosynthesis III, Structure and Molecular Organization of the Photosynthetic Apparatus. G. Akoyunoglou,

editor. Balaban International Science Services, Philadelphia, PA. 15–22.

45. Simpson, D. J. 1982. Freeze-fracture studies on Barley plastid membranes V. Viridis-n34, a photosystem I mutant. *Carlsberg Res. Commun.* 47:215–225.

46. Miller, K. R. 1980. A chloroplast membrane lacking Photosystem I. Changes in unstacked membrane regions. *Biochim. Biophys. Acta.* 592:143–152.

47. Liljenberg, C., G. Wachmeister, and G. Oquist. 1981. Interaction of PQ and α-tocopherol with chloroplast acyl lipids on monomolecular films. *In* Proceedings of the Fifth International Congress on Photosynthesis. G. A. Akoyunoglou, editor. Babalan, Philadelphia, PA. 235–242.

48. Gounaris, K., A. P. R. Brian, P. J. Quinn, and W. P. Williams. 1984. Structural reorganization of chloroplast thylakoid membranes in response to heat-stress. *Biochim. Biophys. Acta.* 766:198–208.

49. Malkin, S. 1968. Kinetic studies on electron-transport components in isolated chloroplasts. I. The effect of the pool of electron carriers between the two photosystems on P700 changes. *Biochim. Biophys. Acta.* 162:392–401.

50. Haehnel, W., and A. Trebst. 1982. Localization of electron transport inhibition in plastoquinone reactions. *J. Bioenerg. Biomembr.* 14:181–190.

51. Forbush, B., B. Kok, and M. P. McGloin. 1971. Cooperation of charges in photosynthetic O_2 evolution.—II. Damping of flash yield oscillation, deactivation. *Photochem. Photobiol.* 14:307–321.

52. Bowes, J. M., and A. R. Crofts. 1980. Binary oscillations in the rate of reoxidation of the primary acceptor of photosystem II. *Biochim. Biophys. Acta.* 590:373–384.

53. Barber, J., R. C. Ford, R. A. C. Mitchell, and P. A. Millner. 1984. Chloroplast thylakoid membrane fluidity and its sensitivity to temperature. *Planta.* 161:375–380.

54. Mauro, S., R. Lannoye, R. Vandeloise, and E. Van der Donckt. 1986. Simulation of the reduction kinetics of P-700$^+$ after flash excitation. *Photobiochem. Photobiophys.* 11:83–94.

55. Fato, R., M. Battino, M. D. Esposti, G. P. Castelli, and G. Lenaz. 1986. Determination of partition and lateral diffusion coefficients of ubiquinones by fluorescence quenching of *n*-(9-anthroyloxy)-stearic acids in phospholipid vesicles and mitochondrial membranes. *Biochemistry.* 25:3378–3390.

56. Millner, P. A., D. J. Chapman, and J. Barber. 1984. The effect of chloroplast coupling factor ATP synthetase (CF1·CF0) reconstitution on fluidity properties of isolated thylakoid lipid vesicles. *Biochim. Biophys. Acta.* 765:282–287.

57. Venturoli, G., J. G. Fernandez-Velasco, A. R. Crofts, and B. A. Melandri. 1986. Demonstration of a collision interaction of ubiquinol with the ubiquinol-cytochrome c2 oxidoreductase complex in chromatophores from *Rhodobacter sphaeroides. Biochim. Biophys. Acta.* 851:340–352.

58. Wang, Z., E. A. Berry, and A. R. Crofts. 1987. Electron transfer from quinol to cytochrome b-561 is not diffusion limited in the ubiquinol:cyt c2 oxidoreductase complex of *Rps. sphaeroides. In* Progress in Photosynthesis Research. J. Biggins, editor. Martinus Nijhoff, Dordrecht, The Netherlands. 2:493–496.

59. Bergström, J., L.-E. Andréasson, and T. Vänngård. 1986. A pre-steady-state kinetic study of electron transfer in the isolated cytochrome bf complex from spinach. *Biochim. Biophys. Acta.* 852:112–118.

60. Hurt, E., and G. Hauska. 1981. A cytochrome f/b_6 complex of five polypeptides with plastoquinol-plastocyanin-oxidoreductase activity from spinach chloroplasts. *Eur. J. Biochem.* 117:591–599.

61. Crofts, A. R., and Z. Wang. 1989. How rapid are the internal reactions of the ubiquinol-cytochrome *c* oxidoreductase? *Photosynth. Res.* 22:69–87.

62. Joliot, P., J. Lavergne, and D. Béal. 1990. Organization of the plastoquinone pool in chloroplasts: evidence for clusters of different sizes. *In* Current Research in Photosynthesis. M. Baltscheffsky, editor. Kluwer Academic Publishers, Dordrecht, The Netherlands. 2:879–882.